ELSEVIER

Contents lists available at ScienceDirect

Chemical Engineering Journal

journal homepage: www.elsevier.com/locate/cej



Short Communication

Enhancing plasma-based cracking of NH₃: The beneficial effect of N₂ versus the detrimental effect of H₂

Seunghwan Bang a,b,*, Ramses Snoeckx a,c

- a CERP, Physical Science and Engineering Division (PSE), King Abdullah University of Science and Technology (KAUST), Thuwal, 23955, Saudi Arabia
- ^b Research Group PLASMANT, Department of Chemistry, University of Antwerp, BE-2610, Antwerp, Belgium
- ^c Plasma & Coating Group, Empa Swiss Federal Laboratories for Materials Science and Technology, Lerchenfeldstrasse 5, 9014, St. Gallen, Switzerland

ARTICLE INFO

Keywords: Plasma Plasma chemical kinetics NH3 cracking Hydrogen production Plasma-catalysis Membrane reaction

ABSTRACT

Hydrogen is a vital energy carrier to decarbonize hard-to-electrify sectors. However, its storage and transport remain challenging. Hence, hydrogen-carriers—chemicals and materials that are hydrogen-rich and easier to store and transport—offer a potential solution. Ammonia stands out due to its carbon-free nature and existing global infrastructure, nevertheless its potential relies on the development of low-cost, high-purity cracking technology. Non-thermal plasmas offer a promising electron-driven approach to achieve this. Previous studies already demonstrated its feasibility, but were typically limited to low conversions. However, for practical applications achieving near-complete conversion to produce high-purity hydrogen is essential. Combined experiments and simulations can provide critical insights into the chemical reaction pathways. Here, we show how the cracking products influence the cracking performance starting from pure ammonia to near-complete conversion. While nitrogen enhances cracking performance, hydrogen hinders it. Based on these findings we propose strategies to exploit these insights and improve cracking efficiency.

1. Introduction

As a carbon-free energy carrier, hydrogen (H₂) is set to play an essential role in achieving a sustainable energy future. Hydrogen will be particularly vital for decarbonizing hard-to-electrify, energy-intensive sectors due to its zero greenhouse gas emissions at the point of use. However, hydrogen's physical properties pose significant challenges for storage and transportation. In its pure form, hydrogen requires either extreme compression or liquefaction at cryogenic temperatures, both of which are energy-intensive and costly [1].

A potential solution involves converting hydrogen into ammonia (NH $_3$) at its point of origin, transporting ammonia, and cracking it back into hydrogen at its point of use. Ammonia is easier to store and transport due to its high energy density (cf. at liquid phase, 15.6 MJ/L for NH $_3$ vs 9.1 MJ/L for H $_2$), liquid state at moderate pressures (7.5 bar, while H $_2$ can't be liquified by adjusting pressure) and temperatures (cf. 240 K for NH $_3$ vs 20 K for H $_2$), and established global infrastructure. One should keep in mind, however, that ammonia poses other challenges due to its toxicity [2]. Nevertheless, for this approach to be viable, the combined efficiency of the conversion, transport, and cracking steps

must surpass alternative methods.

To achieve this, the final cracking step must be energy efficient and produce high-purity hydrogen, ideally powered by renewable energy. Non-thermal plasma is a promising approach as it can activate gas-phase chemical reactions through energetic electrons, independent of gas temperature, in low-cost reactors without the need for expensive catalysts [3-6]. Plasma technology offers a unique opportunity; it is highly flexible, operating across a broad temperature range (from ambient to tens of thousands of Kelvin) with a large reactive volume. Unlike electrochemical methods, plasma systems can be switched on and off instantly, eliminating the need for lengthy preheating [7] and thereby making them compatible with intermittent renewable energy sources. Furthermore, plasma processes differ from conventional thermal methods in their ability to operate under various temperature regimes, where the process is controlled by electron-driven reactions (determined by the electron temperature, T_e); thermally-driven reactions (determined by the gas temperature, T_g); or a combination of both [8–11]. Additionally, in contrast to catalysis, which is limited by the available surface area, often of rare-earth materials, plasma processes occur in the bulk gas phase, lowering the reactor cost and dramatically increasing

E-mail address: seunghwan.bang@uantwerp.be (S. Bang).

^{*} Corresponding author at: CERP, Physical Science and Engineering Division (PSE), King Abdullah University of Science and Technology (KAUST), Thuwal, 23955, Saudi Arabia.

the available reactive volume [3]. These characteristics make plasma processing an ideal Power-to-X (P2X) technology to convert renewable electricity into value-added products matched to the variable output of renewable energy sources. This in turn makes its economics appealing, on both large and small modular scales [4,12].

Prior studies made significant progress in revealing the various reaction pathways involved in the plasma-based NH₃ cracking process to produce N₂ and H₂ [13–17]. Additionally, several studies have successfully explored the opposite process, plasma-based NH₃ synthesis from N₂ and H₂ [18–22]. Even for the thermodynamic nonequilibrium conditions in a plasma, chemical equilibrium principles will dynamically balance NH₃ synthesis from N₂/H₂, and NH₃ decomposition into N₂/H₂, depending on the operating conditions. Hence, understanding how NH₃ conversion evolves from pure NH₃ to a cracked NH₃/N₂/H₂ mixture is crucial for optimizing the process.

We investigated H_2 production rates and NH_3 conversion for varying mixtures: (i) $NH_3/N_2/H_2$ with N_2/H_2 mimicking the 1:3 cracking ratio, (ii) NH_3/N_2 , and (iii) NH_3/H_2 . These mixtures represent plasma-based ammonia cracking: (i) without intervention, (ii) with selective removal of H_2 and (iii) with selective removal of N_2 . Herein, we demonstrate how the cracking products, N_2 and H_2 , affect the plasma-based cracking process—both individually and combined—when progressing from pure ammonia to the nearly completely cracked mixture. Additionally, through 0D plasma chemical kinetics modeling, we revealed underlying chemistry that causes distinct cracking behaviors in various mixture conditions. Finally, we present a brief outlook for the future development of plasma-based ammonia cracking by asking: how can we enhance plasma-based ammonia cracking performance at high conversions (low NH_3 concentration in the mixture)? Here, our findings demonstrates that in-situ H_2 removal and/or N_2 recirculation will be

essential to maintain a stable H_2 production rate and low energy cost throughout the process.

2. Results and discussion

The reference $\rm H_2$ production rate for pure NH₃ is 7.2 NmL/min (star, Fig. 1). For the NH₃/N₂/H₂ mixture (fixed N₂:H₂ ratio of 1:3) (black circles, Fig. 1), this rate decreases significantly when the NH₃ concentration is lowered. Upon initially lowering the NH₃ concentration to 90 %, the H₂ production rate drops to 4.3 NmL/min, followed by a steady decrease to 2.9 NmL/min at 50 %, and a slightly stronger decrease to 0.6 NmL/min at 10 %. The NH₃/H₂ mixture (blue circles, Fig. 1) exhibits a similar trend albeit with slightly lower H₂ production rates: 3.9 NmL/min at 90 %, 2.8 NmL/min at 50 %, and 0.3 NmL/min at 10 %. Hence, both the NH₃/N₂/H₂ and NH₃/H₂ mixtures exhibit diminishing performance as NH₃ cracking progressed from 0 to 90 %.

The NH $_3$ /N $_2$ mixture (red circles, Fig. 1) behaves dynamically. Initially, the H $_2$ production rate is halved to 3.4 NmL/min at 75 %, similar to the other mixtures. However, the decrease is less pronounced, with an initial rate of 5.1 NmL/min at 90 %—the highest among the three. After this initial decline, the H $_2$ production rate nearly completely recovers, reaching 6.7 NmL/min at 25 %. Upon further lowering the NH $_3$ concentration, although decreasing again, the rate remained significantly higher compared to the other mixtures: 4.6 NmL/min at 10 %—about 8 times higher than the NH $_3$ /N $_2$ /H $_2$ mixture and 15 times higher than the NH $_3$ /H $_2$ mixture. Hence, the NH $_3$ /N $_2$ mixture exhibits superior performance compared to the NH $_3$ /N $_2$ /H $_2$ and NH $_3$ /H $_2$ mixtures, especially for NH $_3$ concentrations \leq 50 % (probably even extending to <65–70 %, similar as reported by Mlotek et al. [23]). This can be regarded as a composition-dependent regime (gray-shaded area).

H₂ production rate (NmL/min)

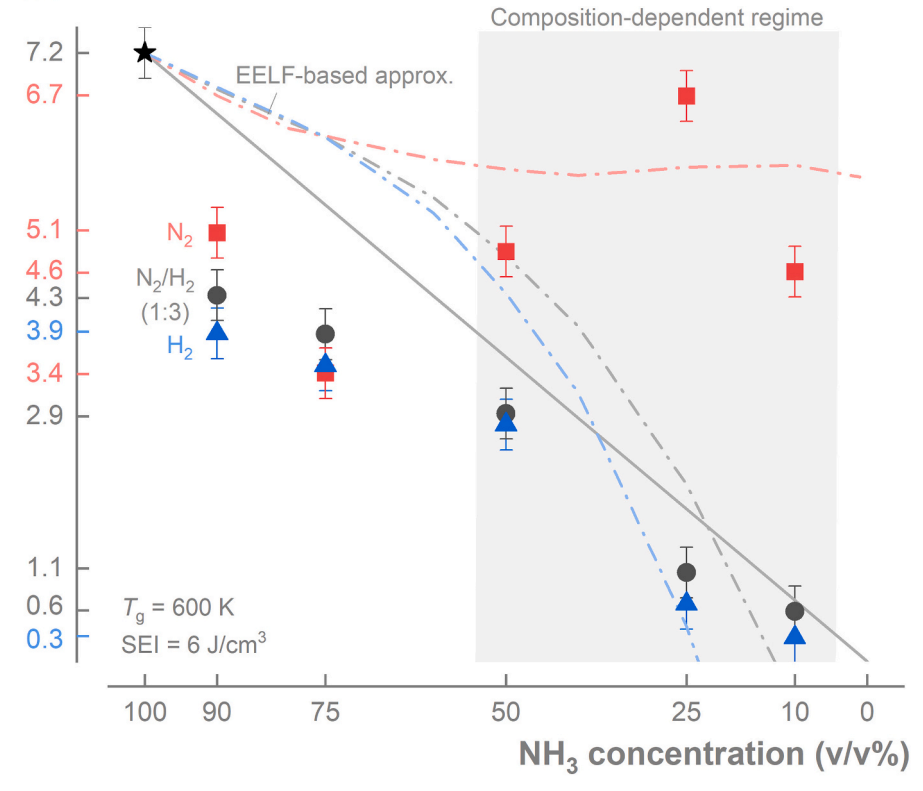


Fig. 1. The measured H_2 production rate generally decreases as the initial NH_3 concentration is lowered. Initially, the three mixtures behave similarly up to the composition-dependent regime. In this regime, the H_2 production rate for NH_3/H_2 and $NH_3/N_2/H_2$ (fixed $N_2:H_2$ ratio of 1:3) continues to decline, whereas that for NH_3/N_2 recovers. A linear dilution approximation (solid line) indicates which mixtures have a positive or negative contribution, whereas an electron energy loss fraction (EELF)-based approximation (dash-dotted line) succeeds in capturing the differences between the mixtures.

The better performance of the NH₃/N₂ mixture is further highlighted when evaluating one of the main parameters for process optimization, the energy cost (see SI for details). For the conditions mimicking the start of the process (pure NH₃), the energy cost is 58 eV/molecule-NH₃. While for the conditions mimicking the end of the process (only 10 % NH₃ in the mixture), this value rises to 709 eV/molecule-NH₃ for the NH₃/N₂/H₂ mixture and to 1488 eV/molecule-NH₃ for the NH₃/H₂ mixture. In contrast, the NH₃/N₂ mixture requires only 91 eV/molecule-NH₃ for 10 % NH₃ in the mixture, while for 25 % NH₃ in the mixture, the energy cost of 62 eV/molecule-NH3 is even comparable to the pure NH3 conditions (58 eV/molecule-NH₃). Hence, for continuous operation from pure NH₃ down to low concentrations (up to 10 % in this study), the average energy cost for NH₃/N₂ (84 eV/molecule-NH₃) is approximately three times lower compared to NH $_3/N_2/H_2$ (252 eV/molecule-NH₃) and about five times lower compared to NH₃/H₂ (424 eV/molecule-NH₃).

The obtained energy costs are comparable to those reported in literature for DBDs (e.g. 85 eV/molecule-NH3 with packed-bed DBD [24] and 143 eV/molecule-NH₃ with Cu-catalysts-loaded DBD [25], see Table 1). Additionally, as is clear from the available data in literature (Table 1), pin-to-pin, non-thermal arc plasma jet (NTAP) and gliding arc (GA) reactors operating at relatively high gas temperatures (~3000 K) outperform DBDs when evaluated in terms of energy cost. Among others, this is a consequence of the difference in activation energy between electron-induced (threshold energy, E_{th}) and thermally driven (reaction enthalpy, $\Delta H_{\rm r}$) reactions [11,26], with the former dominating in low-temperature plasmas (e.g. DBD, radio frequency (RF), Corona) and the latter in warmer plasmas (e.g. NTAP, GA, MW). Hence, future work should explore whether the effects of different mixture compositions observed here for low-temperature plasmas are also valid for plasmas operating at higher gas temperatures (and typically lower reduced electric fields).

Regardless of traditional chemical equilibrium considerations, it is not surprising that a lower NH_3 concentration leads to a reduced H_2 production rate and increased energy cost. In plasma-based gas conversion, energy is distributed across the entire gas volume (i.e. SEI) [11]. When the NH_3 concentration decreases, less energy is transferred to NH_3 , while more is transferred to NL_2 and HL_2 . As a first approximation, if NL_3 is only cracked proportional to the supplied energy, and the energy supplied to NL_2 and HL_2 is not transferred to processes that can contribute to cracking of NL_3 , then we can represent the expected decrease in NL_2 production rate through a linear function that reaches 0 NL_2 min at 0 vol% NL_3 (gray solid line, Fig. 1). Deviations from this case then indicate that at least part of the energy supplied to NL_2 and HL_2 contributes to reactions that do affect the cracking process. In general, the values for $\mathrm{NL}_3/\mathrm{HL}_2$ and $\mathrm{NL}_3/\mathrm{NL}_2/\mathrm{HL}_2$ are clearly below this linear approximation,

Table 1Energy cost of NH3 cracking obtained with various plasma reactors.

Reactor type	Gas composition	Gas temperature (K)	Energy cost (eV/molecule- NH ₃)	Ref.
DBD	100 % NH ₃	600	58	This
	$10 \% NH_3 in N_2$	600	91	work
	10 % NH ₃ in	600	709	
	$N_2/H_2(1:3)$			
	10% NH $_3$ in H $_2$	600	1488	
Packed-bed DBD	100 % NH ₃	300	84	[24]
DBD with Cu- catalysts	5 % NH ₃ in N ₂	523	143	[25]
RF Plasma	1 % NH3 in Ar	315-600	20-50	[15]
Non-thermal Arc Plasma jet (NTAP)	100 % NH ₃	1116	1.6	[27]
Pin-to-pin plasma	100 % NH ₃	-	1.5	[28]
Gliding Arc Plasmatron (GAP)	100 % NH ₃	-	2.19	

whereas that for NH_3/N_2 is above it. This indicates that the energy transferred into electron-collisions with H_2 is contributing to processes that counteract NH_3 conversion, while the energy transferred into electron-collisions with N_2 is contributing to processes that enhance NH_3 conversion. This is in line with findings in literature where gases such as Ar, He, and N_2 have a beneficial effect through their highly energetic metastable states [13,14,29,30].

However, the energy transferred to NH $_3$, N $_2$, and H $_2$ is not directly proportional to its concentration but depends on the threshold energies and cross-sections of the various electron-neutral collision processes. A more accurate approximation relies on calculating the fraction of electron energy lost—or rather supplied—to the specific processes that are influencing the cracking efficiency for each individual mixture (dashdotted lines Fig. 1) using their cross-section data [31,32] and a Boltzmann solver (e.g. Bolsig+ [33]). The processes considered are NH $_3$ dissociation (positive contribution), N $_2$ electronic excitation (positive contribution), and H $_2$ dissociation (negative contribution). For more details see Section S3 in the SI.

This electron energy loss fraction (EELF)-based approximation captures the differences in behavior of the three mixtures remarkably well. At NH $_3$ concentrations $\geq 75~\nu/v\%$, the H $_2$ production rate remains nearly identical across all three mixtures. Below this threshold, the NH $_3/N_2$ mixture (red dash-dotted line, Fig. 1) exhibits only a minor decrease, followed by a near constant H $_2$ production rate $> 5.7~\rm NmL/min$ up to 1- $\nu/v\%$ NH $_3$. In contrast, the NH $_3/H_2$ (blue dash-dotted line, Fig. 1) and NH $_3/N_2/H_2$ (gray dash-dotted line, Fig. 1) mixtures exhibit a dramatic decrease, with H $_2$ production dropping to 0 NmL/min at 13 and 23 v/v% NH $_3$, respectively. This highlights that, besides electron impact dissociation of NH $_3$, H radicals and electronic excited N $_2$ play a key role in the cracking process.

Our results show that the presence of N_2 enhances NH_3 cracking, while H_2 inhibits it. Notably, H_2 's negative impact is stronger than N_2 's positive effect, as $NH_3/N_2/H_2$ performs only slightly better than NH_3/H_2 . This highlights the importance of understanding the underlying dynamics. Successfully leveraging these effects could contribute to improvements in the efficiency of the plasma-based NH_3 cracking process through optimized reactor performance.

To explore the chemical reaction pathways behind the observed trends, we performed 0D plasma-chemical kinetic simulations. We developed an improved version of our previously published temperature-dependent plasma-chemical reaction mechanism [13] and assessed its performance against experimental data for two distinct operating regimes and the same three mixtures with an NH₃ concentration of 1 ν /v%: thermal NH₃ cracking (900 $\leq T_g \leq$ 2300 K and $P_{\rm dis} =$ 0 W; Fig. 2a) and plasma-based NH₃ cracking (300 $\leq T_g \leq$ 900 K and $P_{\rm dis} =$ 20 W, SEI = 1.2 J/cm³; Fig. 2b). In follow-up work, we aim to extend the validity of the mechanism to cover the full range of operating conditions (i.e. NH₃ concentrations and temperature range), however, as outlined in our previous work, this requires the development of more accurate reaction rate and cross section data for several important species [13].

Our improved reaction mechanism showed better performance compared to the previous mechanism (see Section S2.4 in SI) in capturing the experimental trends. For thermal cracking, our simulations effectively captured the shift in conversion onset to higher gas temperatures for $NH_3/N_2/H_2$ and NH_3/H_2 compared to NH_3/N_2 , showing only a minor deviation of the experimental onset temperature for NH_3/N_2 : 1200 K (red line, Fig. 2a) versus 1350 K experimentally (red symbols, Fig. 2a).

For plasma-based cracking, our simulations captured the differences between the mixtures: predicting a negligible conversion for NH $_3$ /H $_2$ consistent with the experiments; for NH $_3$ /N $_2$ /H $_2$ a minor conversion compared to a negligible conversion in the experiments; and for NH $_3$ /N $_2$ an increased NH $_3$ conversion with increased gas temperature (at $T_g \leq 600$ K), followed by a decrease, and gradual increase. In absolute values, the latter displays an underestimation at $T_g < 600$ K, an overestimation

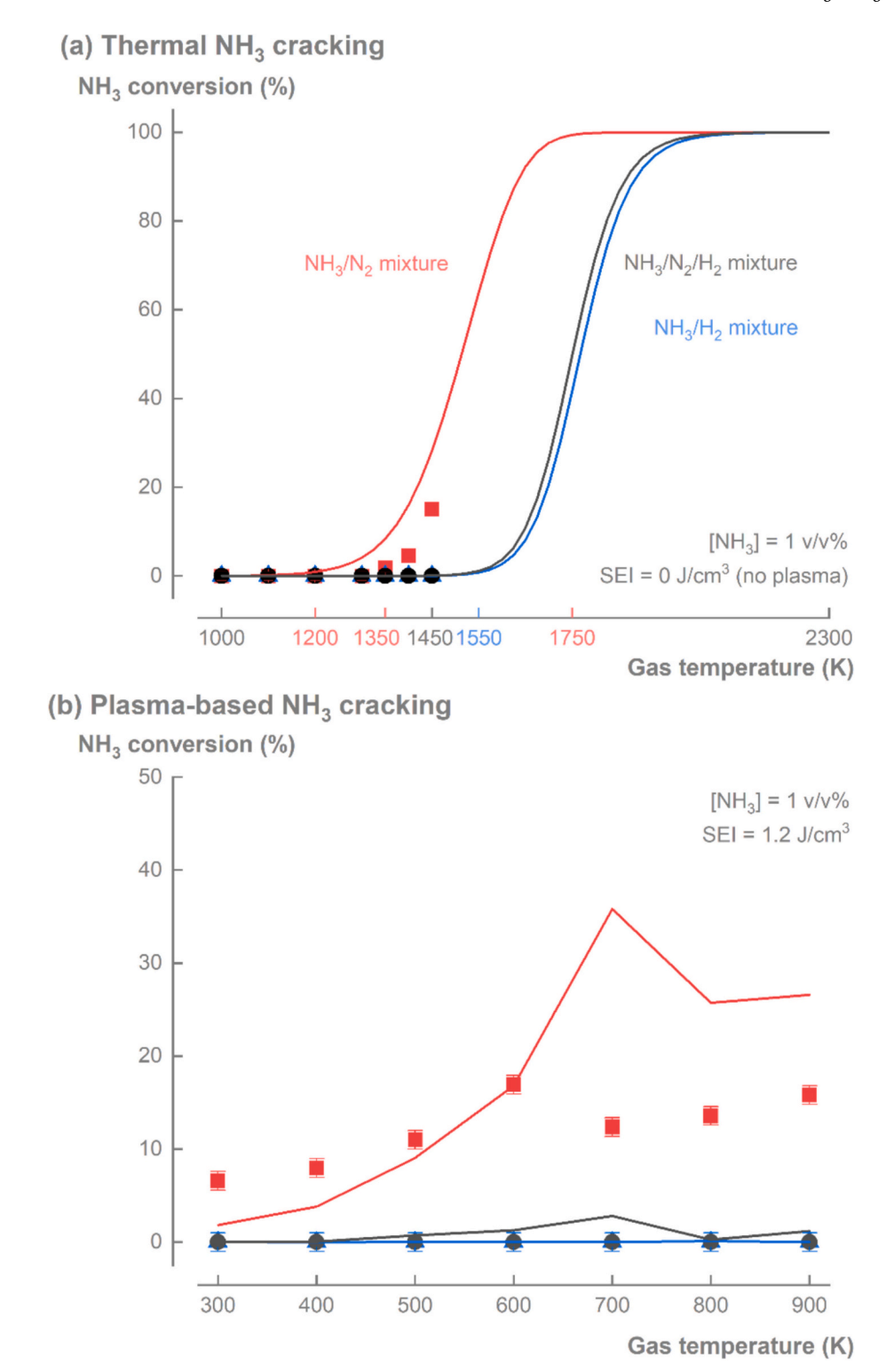


Fig. 2. With an improved plasma-chemical reaction mechanism, the model (lines) captures the experimental trends of NH_3 conversion (symbols) for both (a) thermal and (b) plasma-based NH_3 cracking. For thermal cracking, the conversion onset temperature varies significantly with mixture composition: NH_3/N_2 exhibits the lowest onset temperature (red, 1200 K) compared to $NH_3/N_2/H_2$ (black, 1550 K) and NH_3/H_2 (blue, 1550 K). For plasma-based cracking, NH_3/N_2 shows significant conversions independent of the gas temperature, whereas $NH_3/N_2/H_2$ and NH_3/H_2 show negligible conversions. The maximum attainable gas temperature was limited to 1450 K for the thermal cracking experiments (which was the limit of the electric furnace) and only 900 K for the plasma-based NH_3 cracking experiments (due to discharge instabilities at higher temperatures). Experimental data points for the NH_3/N_2 mixture are reproduced from our previous work [13].

at $T_{\rm g}$ > 600 K, and a shift of 100 K for the peak value. The qualitative match between our experiments and simulations supports using the model to explore the underlying chemical pathways and identify opportunities for optimizing plasma-based ammonia cracking.

Thirteen reactions play a pivotal role throughout the cracking process. Five of those are primarily driving NH $_3$ cracking and recombination. Like other plasma-based gas conversion processes [9,10,34–36], plasma-based NH $_3$ cracking is initiated by collisions with highly

energetic electrons, triggering electron-impact reactions. Due to the low NH $_3$ concentration (1 ν/ν %) and high N $_2/H_2$ concentrations in our simulations, the dominant initiation channels are electron-impact reactions with N $_2$ (R1) and H $_2$ (R4) rather than electron-impact reactions with NH $_3$ (R6). Whereas, the latter are important for studies with higher NH $_3$ concentrations or using Ar as dilutant [15,37], in the present work they have a negligible contribution (see Fig. S23 in the SI).

For the NH_3/N_2 mixture (1:99), the main process is electronic excitation of N_2 (Eq. (R1)):

$$e^- + N_2 \rightarrow e^- + N_2^*$$
 (R1)

 N_2 is excited to eight different excited states (i.e., $N_2(A^3\Sigma_u^+)$, $N_2(B^3\Pi_g)$, $N_2(B^3\Sigma_u^-)$, $N_2(W^3\Delta)$, $N_2(a^1\Pi_g)$, $N_2(a^1\Sigma_u^-)$, $N_2(W^1\Delta)$, $N_2(C^3\Pi_u)$), which mostly relax to the highly energetic meta-stable states $N_2(A^3)$ and $N_2(a^1)$ (see Fig. S19–S21 and Table S15 in SI for details). These meta-stable species subsequently induce NH_3 decomposition via Penning dissociation reactions (R2 and R3):

$$N_2(A^3) + NH_3 \rightarrow NH_2 + H$$
 (R2)

$$N_2(a^1) + NH_3 \rightarrow NH_2 + H$$
 (R3)

Thus, the observed NH_3 conversion primarily results from the indirect energy transfer via these metastable states (on average, 80% of NH_3 decomposition is due to R2, and 14% due to R3, see Fig. S23 in SI). It is important to note that Penning dissociation by other excited states such as $N_2(B^3)$ is negligible, for the conditions investigated (1 $\nu/\nu\%$ NH_3), because under atmospheric pressure, these states are efficiently quenched into lower-lying metastable states through collisions with neutral N_2 and H_2 (Figs. S19–S21). For conditions with low N_2 and H_2 (and high NH_3) concentrations it is possible that Penning dissociation of NH_3 with other metastable states does play a role—due to the low concentration of the non-dissociative quenching partners (N_2 and H_2).

For the NH_3/H_2 mixture (1:99), on the other hand, the main process is the electron impact dissociation of H_2 (Eq. (R4)):

$$e^{-} + H_2 \rightarrow e^{-} + H + H$$
 (R4)

with 84 % of the H radicals recombining to H₂ (Eq. (R5)):

$$H + H (+M) \rightarrow H_2 (+M)$$
 (R5)

In the NH₃/H₂ mixture, there is no strong mechanism for indirect energy transfer leading to NH₃ conversion. Hence, despite its negligible reaction rate, electron impact dissociation of NH₃ (R6) is the main process at low temperatures ($T_{\rm g} < 800$ K):

$$e^{-} + NH_{3} \rightarrow e^{-} + NH_{2} + H$$
 (R6)

Only at $T_8 > 600$ K, H-abstraction reaction involving NH₃ become more significant and contribute to NH₃ conversion (Eq. (R7)):

$$NH_3 + H \rightarrow NH_2 + H_2 \tag{R7}$$

In contrast to pure thermal NH $_3$ cracking, the rates of H-abstraction reactions with NH $_2$ and NH were generally negligible. Only for the NH $_3$ /N $_2$ mixture at $T_{\rm g}=800$ K, H-abstraction with NH $_2$ became relevant (Fig. S16b in SI).

Nevertheless, the recombination of NH₂ with H (Eq. (R8)) competes with Eqs. (R5) and (R7) throughout all low-temperature conditions examined in this study ($T_{\rm g}$ < 900 K):

$$NH_2 + H (+M) \rightarrow NH_3 (+M)$$
 (R8)

This recombination reaction is responsible for undoing any NH_3 conversion in the NH_3/H_2 mixture (and the $NH_3/N_2/H_2$ mixture, see below).

For the $NH_3/N_2/H_2$ mixture (1:24.75:74.25), 17 % of the electron energy is going into R1 versus 48 % into R4 (Fig. S12a), explaining why the mixture behaves more similar to NH_3/H_2 rather than to NH_3/N_2 . Moreover, the metastable states $N_2(A^3)$ and $N_2(a^1)$ contribute to

additional dissociation of H_2 (Eqs. (R9) and (R10)) at the expense of NH_3 dissociation (Eqs. (R2) and (R3)):

$$N_2(A^3) + H_2 \rightarrow N_2 + H + H$$
 (R9)

$$N_2(a^1) + H_2 \rightarrow N_2 + H + H$$
 (R10)

Although the metastable states still enable some indirect energy transfer for NH_3 conversion (Eqs. (R2) and (R3)), the dominant recombination reaction (R8)—supported by the additional production of H radicals (Eqs. (R9) and (R10))—suppress net conversion, similar to the NH_3/H_2 mixture.

The absence of other reactions with notable contributions in the main chemical pathways for NH $_3$ conversion suggests that even for higher NH $_3$ concentrations (Fig. 1), the competition between Penning dissociation (Eqs. (R2) and (R3)) and recombination (Eq. (R8)) is most likely the primary factor for NH $_3$ conversion (and H $_2$ production rate). Additionally, for high N $_2$ concentrations our simulations show electronimpact dissociation of N $_2$ (Eq. (R11)) and the reactions of NH $_2$ with N radicals (Eq. (R12) and (R13)) become important—and thus potentially contributing to the recovery in H $_2$ production rate (and NH $_3$ conversion) between 75 and 10 ν/ν % NH $_3$:

$$e^- + N_2 \rightarrow e^- + N + N$$
 (R11)

$$NH_2 + N \rightarrow N_2 + H + H \tag{R12}$$

$$NH_2 + N \rightarrow N_2 + H_2 \tag{R13}$$

Eq. (R13) generates N radicals that subsequently react with NH $_2$ into N $_2$ and H radicals (Eq. (R12)) or H $_2$ (Eq. (R13)). This reaction introduces a pathway that disrupts the balance between Penning dissociation and recombination (Fig. 3), effectively enhancing the H $_2$ production rate and NH $_3$ conversion for NH $_3$ /N $_2$ mixtures.

Based on these insights, we can start to explore strategies to

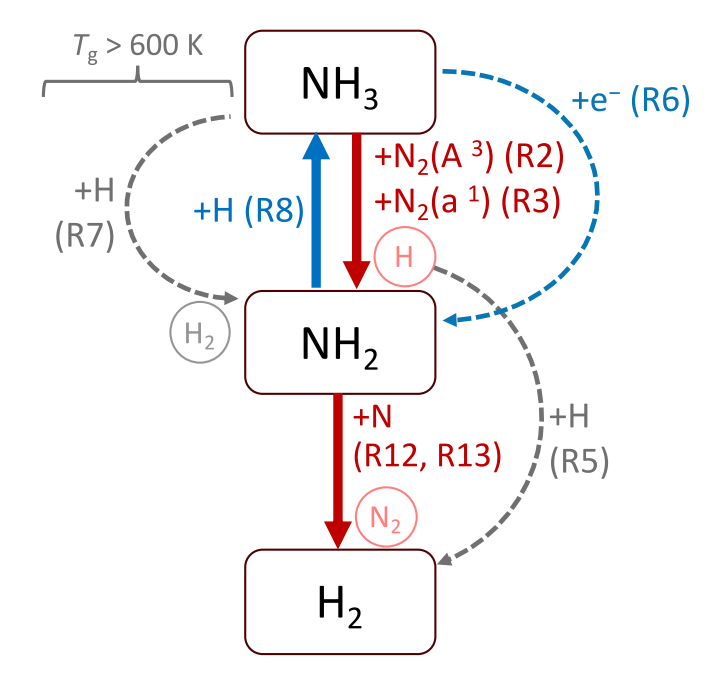


Fig. 3. Although the cracking process is initiated by electron impact reactions, the overall $\rm NH_3$ conversion is predominantly determined by competition between penning dissociation (Eqs. (R2) and (R3)) and recombination (Eq. (R8)). Environments with high $\rm N_2$ concentrations enhance penning dissociation (Eqs. (R2) and (R3)), while reactions between NH2 and N (Eqs. (R12) and (R13)) further facilitate NH3 decomposition (red). Conversely, environments with high H2 concentrations favor recombination reactions (blue). Additionally, at temperatures above 600 K, hydrogen abstraction reaction (Eq. (R7)) becomes significant.

maximize H₂ production efficiency at high NH₃ conversion rates.

The first strategy involves in-situ H_2 removal to minimize recombination (Eq. (R8)), which can be achieved by integrating H_2 -permeable membranes, similar to thermal NH_3 cracking [38]. Beyond mitigating recombination effects (as already attempted by Hayakawa et al. [39]), we must also optimize NH_3 cracking (e.g. via penning dissociation of NH_3 (Eqs. (R2) and (R3)) and electron impact dissociation of N_2 (Eq. (R11))) by controlling the NH_3/N_2 ratio through selective NH_3 or N_2 addition after H_2 removal. This could be achieved through recirculating N_2 and/or uncracked NH_3 . It should be considered, however, that the dominant role of metastable states may only be observed in high-E/N plasmas, such as DBDs and nanosecond pulsed discharges. This could explain why the contribution of Penning dissociation by Ar was absent in RF plasma-based NH_3 cracking with 1 % NH_3 in Ar [15].

A second potential strategy is coupling the plasma with a catalytic material—known as plasma-catalysis [40-44]—to promote the cracking efficiency in a synergistic manner. Plasma-generated vibrational and electronic excited species (via Eq. (R1)) can reduce the activation energy required for NH₃ decomposition on the catalytic surface. However, the choice of catalyst and packing material (e.g., Al₂O₃, BaTiO₃ as supports) requires careful consideration, as they can shift the discharge mode from energetic micro-discharges to diffuse, thereby reducing the contribution of electron-impact dissociation reactions [45]. Deliberate catalyst and support design can yield positive effects—for example, increasing the number of discharge channels [46] or promoting a transition from diffuse to energetic micro-discharges, thereby facilitating dissociation of the strong N₂ bond (via Eq. (R11)) [47]. Both approaches could enhance cracking efficiency and highlight the importance of thoughtful systematic studies on tailored catalyst design. Moreover, although catalyst nitridation by N radicals has been shown to negatively impact conventional NH₃ cracking [48], in plasma-catalysis under low T_g , it could prove beneficial by providing abundant N radicals on the catalytic surface that can facilitate NH2 reactivity (via Eqs. (R12) and (R13)).

A third strategy is using non-thermal plasma reactors operating at higher gas temperatures, $T_{\rm g} > 1500$ K (e.g. microwave and gliding arc discharges), to stimulate thermal decomposition with the heat produced by the discharge [26,27,49,50], with a potential additional efficiency gain due to non-equilibrium effects from the increased entropy [11,26]. Here, it is essential to maximize the transfer of electron energy into gas heating and obtain control over the gas temperature to maximize overall energy efficiency.

Despite these prospects, a key challenge in plasma-based NH_3 cracking remains the limited understanding of reaction kinetics across the broad operating parameter space [13]. Therefore, a parametric study of plasma-based NH_3 cracking for pure NH_3 , coupled with validated kinetics that can be used for self-consistent multidimensional simulations, is pressing. Combined with system analysis at a practical scale, these steps will allow to optimize plasma-based NH_3 cracking and assess its feasibility in facilitating the adoption of NH_3 as a hydrogen carrier.

3. Methods

Experiments were performed in a temperature-controlled dielectric barrier discharge (DBD) reactor [13] and coupled with zero-dimensional (0D) plasma-chemical kinetic simulations using KAUSTKin and an improved temperature-dependent ammonia reaction mechanism (details in Sections S1, S2 and S6 in Supporting Information (SI)).

To examine non-thermal plasma-based NH_3 cracking ranging from pure ammonia at the start to high conversions (90 %), the H_2 production rate (in NmL/min) was experimentally measured for different initial NH_3 concentrations (ranging from 100 to 10 ν/ν %- NH_3). Lowering the NH_3 concentration mimics the continuous progress of the cracking process under fixed conditions, allowing us to systematically assess the H_2 production rate without changing operating conditions (e.g. flow rate, power, specific energy input (SEI)). Additionally, three different mixtures were used to evaluate both the combined effect of N_2 and H_2 , as

well as their individual effects on the process: (i) NH₃/N₂/H₂ with N₂/H₂ reflecting the stoichiometric 1:3 cracking ratio, (ii) NH₃/N₂, and (iii) NH₃/H₂ (Fig. 1). The chosen gas temperature ($T_{\rm g}=600~{\rm K}$) and discharge power ($P_{\rm dis}=20~{\rm W}$, corresponding to SEI = 6 J/cm³) showed the best performance in our previous work [13].

For 0D plasma-chemical kinetic simulations, the temperature-dependent ammonia reaction mechanism was implemented in 0D kinetics solver called KAUSTKin and benchmarked against the full set of experimental data. Simulations were performed across the same temperature window explored experimentally (300–900 K), at 1 v/v%-NH₃, and for the three feed-gas configurations detailed above—NH₃/N₂/H₂ with the stoichiometric N₂:H₂ = 1:3 ratio, NH₃/N₂, and NH₃/H₂. This unified framework confirms that the mechanism reliably reproduces the combined and individual effects of N₂ and H₂ on plasma-assisted NH₃ cracking over the entire range of operating temperatures.

Affiliation statement

Most of the work was performed at King Abdullah University of Science and Technology (KAUST) (i.e. Conceptualization and Methodology, Investigation, Formal analysis and Visualization), part of the work was performed at Empa, Swiss Federal Laboratories for Materials Science and Technology, and University of Antwerp (i.e. Formal analysis and Visualization, and Writing).

CRediT authorship contribution statement

Seunghwan Bang: Writing – original draft, Visualization, Software, Methodology, Investigation, Formal analysis, Data curation, Conceptualization. **Ramses Snoeckx:** Writing – review & editing, Visualization, Supervision, Methodology, Formal analysis, Conceptualization.

Declaration of competing interest

The authors declare that they have no known competing financial interests or personal relationships that could have appeared to influence the work reported in this paper.

Acknowledgment

The research reported in this work was funded by King Abdullah University of Science and Technology (KAUST) under award number BAS/1/1384-01-01.

Appendix A. Supplementary data

Supplementary data to this article can be found online at https://doi. org/10.1016/j.cej.2025.169738.

Data availability

The data supporting this article have been included as part of the Supplementary Information.

References

- S. Niaz, T. Manzoor, A.H. Pandith, Hydrogen storage: materials, methods and perspectives, Renew. Sustain. Energy Rev. 50 (2015) 457–469, https://doi.org/ 10.1016/j.rser.2015.05.011.
- [2] Y. Kojima, Safety of Ammonia as a hydrogen energy carrier, Int. J. Hydrogen Energy 50 (2024) 732–739, https://doi.org/10.1016/j.ijhydene.2023.06.213.
- [3] R. Snoeckx, A. Bogaerts, Plasma technology-a novel solution for CO2 conversion? Chem. Soc. Rev. 46 (19) (2017) 5805–5863, https://doi.org/10.1039/c6cs00066e.
- [4] A. Bogaerts, E.C. Neyts, Plasma technology: an emerging Technology for Energy Storage, ACS Energy Lett. 3 (4) (2018) 1013–1027, https://doi.org/10.1021/ acsenergylett.8b00184.
- [5] A. Bogaerts, Plasma technology for the electrification of chemical reactions, Nat Chem Eng (2025), https://doi.org/10.1038/s44286-025-00229-3.

- [6] O.I. Awad, B. Zhou, K. Kadirgama, Z. Chen, M.N. Mohammed, Nonthermal plasmaassisted catalysis NH3 decomposition for COx-free H2 production: a review, Int. J. Hydrogen Energy 56 (2024) 452–470, https://doi.org/10.1016/j. iibvdene 2023 12 166
- [7] I. Adamovich, S. Agarwal, E. Ahedo, L.L. Alves, S. Baalrud, N. Babaeva, A. Bogaerts, A. Bourdon, P.J. Bruggeman, C. Canal, E.H. Choi, S. Coulombe, Z. Donkó, D.B. Graves, S. Hamaguchi, D. Hegemann, M. Hori, H.-H. Kim, G.M. W. Kroesen, M.J. Kushner, A. Laricchiuta, X. Li, T.E. Magin, S.M. Thagard, V. Miller, A.B. Murphy, G.S. Oehrlein, N. Puac, R.M. Sankaran, S. Samukawa, M. Shiratani, M. Šimek, N. Tarasenko, K. Terashima, E. T. Jr., J. Trieschmann, S. Tsikata, M.M. Turner, I.J. van der Walt, M.C.M. van de Sanden, T. von Woedtke, The 2022 plasma roadmap: low temperature plasma science and technology, J. Phys. D Appl. Phys. 55 (37) (2022) 373001, https://doi.org/10.1088/1361-6463/ac5e1c.
- [8] M.S. Cha, R. Snoeckx, Plasma technology-preparing for the electrified future, Front. Mech. Eng. 8 (2022).
- [9] S. Bang, R. Snoeckx, M.S. Cha, Temperature-dependent kinetics of ozone production in oxygen discharges, Plasma Chem Plasma Process (2023), https://doi. org/10.1007/s11090-023-10370-7.
- [10] A. Mohanan, R. Snoeckx, M.S. Cha, Temperature-dependent kinetics of plasmabased CO₂ conversion: interplay of electron-driven and thermal-driven chemistry, ChemSusChem (2024) e202401526, https://doi.org/10.1002/cssc.202401526.
- [11] D. Hegemann, P. Navascués, R. Snoeckx, Plasma gas conversion in non-equilibrium conditions, Int. J. Hydrogen Energy 100 (2025) 548–555, https://doi.org/ 10.1016/j.jihydene.2024.12.351.
- [12] J. Osorio-Tejada, N.N. Tran, V. Hessel, Techno-environmental assessment of small-scale Haber-Bosch and plasma-assisted ammonia supply chains, Sci. Total Environ. 826 (2022) 154162, https://doi.org/10.1016/j.scitotenv.2022.154162.
- [13] S. Bang, R. Snoeckx, M.S. Cha, Kinetic study for plasma assisted cracking of NH3: approaches and challenges, J. Phys. Chem. A (2023), https://doi.org/10.1021/acs. jpca.2c06919.
- [14] S. Li, H. Guo, G. Yin, E. Hu, Z. Huang, Experimental and kinetic study of non-equilibrium plasma driven NH3 decomposition, Fuel 405 (2026) 136427, https://doi.org/10.1016/j.fuel.2025.136427.
- [15] B.N. Bayer, A. Bhan, P.J. Bruggeman, Reaction pathways and energy consumption in NH3 decomposition for H2 production by low temperature, atmospheric pressure plasma, Plasma Chem. Plasma Process. 44 (6) (2024) 2101–2118, https:// doi.org/10.1007/s11090-024-10501-8.
- [16] Y. Gao, M. Zhou, E. Hu, Y. Zhao, G. Yin, Z. Huang, Hydrogen generation by dielectric barrier discharge plasma assisted ammonia decomposition, Energ. Conver. Manage. 306 (2024) 118271, https://doi.org/10.1016/j. enconman.2024.118271.
- [17] R. Robert, F. Massines, L. Stafford, NH3 dissociation along the gas flow lines of Ar-NH3 dielectric barrier discharges and its effects on global and local properties, J. Phys. D Appl. Phys. 58 (26) (2025) 265206, https://doi.org/10.1088/1361-6463/ade1e5
- [18] P. Mehta, P. Barboun, F.A. Herrera, J. Kim, P. Rumbach, D.B. Go, J.C. Hicks, W. F. Schneider, Overcoming ammonia synthesis scaling relations with plasmaenabled catalysis, Nat. Catal. 1 (4) (2018) 269–275, https://doi.org/10.1038/s41929-018-0045-1
- [19] L.R. Winter, B. Ashford, J. Hong, A.B. Murphy, J.G. Chen, Identifying surface reaction intermediates in plasma catalytic ammonia synthesis, ACS Catal. 10 (24) (2020) 14763-14774. https://doi.org/10.1021/acceptal.0c03166
- (2020) 14763–14774, https://doi.org/10.1021/acscatal.0c03166.
 [20] H. Zhao, G. Song, Z. Chen, X. Yang, C. Yan, S. Abe, Y. Ju, S. Sundaresan, B.E. Koel, In situ identification of NNH and N2H2 by using molecular-beam mass spectrometry in plasma-assisted catalysis for NH3 synthesis, ACS Energy Lett. 7 (1) (2022) 53–58, https://doi.org/10.1021/acsenergylett.1c02207.
- [21] T. Zhang, R. Zhou, S. Zhang, R. Zhou, J. Ding, F. Li, J. Hong, L. Dou, T. Shao, A. B. Murphy, K. (Ken) Ostrikov, P.J. Cullen, Sustainable ammonia synthesis from nitrogen and water by one-step plasma catalysis, Energy Environ. Mater. 6 (2) (2023) e12344, https://doi.org/10.1002/eem2.12344.
- [22] C. Ndayirinde, Y. Gorbanev, R.-G. Ciocarlan, R. De Meyer, A. Smets, E. Vlasov, S. Bals, P. Cool, A. Bogaerts, Plasma-catalytic Ammonia synthesis: packed catalysts act as plasma modifiers, Catal. Today 419 (2023) 114156, https://doi.org/ 10.1016/j.cattod.2023.114156.
- [23] M. Mlotek, M. Perron, K. Krawczyk, Ammonia decomposition in a gliding discharge plasma, Energ. Technol. (2021), https://doi.org/10.1002/ente.202100677.
- [24] P. Navascués, J.M. Obrero-Pérez, J. Cotrino, A.R. González-Elipe, A. Gómez-Ramírez, Unraveling discharge and surface mechanisms in plasma-assisted Ammonia reactions, ACS Sustain. Chem. Eng. 8 (39) (2020) 14855–14866, https://doi.org/10.1021/acssuschemeng.0c04461.
- [25] M. Akiyama, K. Aihara, T. Sawaguchi, M. Matsukata, M. Iwamoto, Ammonia decomposition to clean hydrogen using non-thermal atmospheric-pressure plasma, Int. J. Hydrogen Energy 43 (31) (2018) 14493–14497, https://doi.org/10.1016/j. ijhydene.2018.06.022.
- [26] Ramses Snoeckx; Hegemann, D. Entropy export in plasmas an authors' view. Plasma Process. Polym. Under Review.
- [27] Q.F. Lin, Y.M. Jiang, C.Z. Liu, L.W. Chen, W.J. Zhang, J. Ding, J.G. Li, Instantaneous hydrogen production from ammonia by non-thermal arc plasma combining with catalyst, Energy Rep. 7 (2021) 4064–4070, https://doi.org/ 10.1016/j.egyr.2021.06.087.
- [28] I. Fedirchyk, I. Tsonev, R. Quiroz Marnef, A. Bogaerts, Plasma-assisted NH3 cracking in warm plasma reactors for green H2 production, Chem. Eng. J. 499 (2024) 155946, https://doi.org/10.1016/j.cej.2024.155946.

- [29] R. Snoeckx, M.S. Cha, Inevitable chemical effect of balance gas in low temperature plasma assisted combustion, Combust. Flame 225 (2021) 1–4, https://doi.org/ 10.1016/j.combustflame.2020.10.028.
- [30] A. Fateev, F. Leipold, Y. Kusano, B. Stenum, E. Tsakadze, H. Bindslev, Plasma chemistry in an atmospheric pressure Ar/NH3 dielectric barrier discharge, Plasma Processes Polym. 2 (3) (2005) 193–200, https://doi.org/10.1002/ ppap.200400051.
- [31] R. Snoeckx, J. Tennyson, M.S. Cha, Theoretical cross sections for electron collisions relevant for ammonia discharges part 1: NH3, NH2, and NH, Plasma Sources Sci. Technol. 32 (11) (2023) 115020, https://doi.org/10.1088/1361-6595/ad0d07.
- [32] S.B. Pancheshnyi, S. F., Marie-Claude Bordage, Gerjan Hagelaar, W.L. Morgan, A. V. Phelps, Leanne Pitchford, The LXCat project: electron scattering cross sections and swarm parameters for low temperature plasma modeling, Chem. Phys. 398 (398) (2012) 148–153, https://doi.org/10.1016/j.chemphys.2011.04.020.
- [33] G.J.M. Hagelaar, L.C. Pitchford, Solving the Boltzmann equation to obtain Electron transport coefficients and rate coefficients for fluid models, Plasma Sources Sci. Technol. 14 (4) (2005) 722–733, https://doi.org/10.1088/0963-0252/14/4/011.
- [34] Snoeckx, R.H. Stijn, K. Van Wesenbeeck, Silvia Lenaerts, Annemie Bogaerts, CO2 conversion in a dielectric barrier discharge plasma: N2 in the mix as a helping hand or problematic impurity? Energ. Environ. Sci. 9 (3) (2016) 999–1011, https://doi.org/10.1039/c5ee03304g.
- [35] M. Shen, W. Guo, L. Tong, L. Wang, P.K. Chu, S. Kawi, Y. Ding, Non-thermal plasma driven dry reforming of methane: electron energy-input power coupling mechanism and catalyst design criteria, Front. Chem. Sci. Eng. 19 (9) (2025) 84, https://doi.org/10.1007/s11705-025-2596-4.
- [36] B. Zhang, H. Zuo, B. Wu, K. Kamiya, L. Ma, N. Kobayashi, Y. Ma, T. Jin, Y. Chen, Recent Progress in CO2 splitting processes with non-thermal plasma-assisted, J. Environ. Chem. Eng. 12 (6) (2024) 114692, https://doi.org/10.1016/j. iece. 2024.114692
- [37] R.A. Arakoni, A.N. Bhoj, M.J. Kushner, H2 generation in Ar/NH3 microdischarges, J. Phys. D Appl. Phys. 40 (8) (2007) 2476, https://doi.org/10.1088/0022-3727/ 40/8/010.
- [38] J.L. Cerrillo, N. Morlanés, S.R. Kulkarni, N. Realpe, A. Ramírez, S.P. Katikaneni, S. N. Paglieri, K. Lee, A. Harale, B. Solami, A. Jamal, S. Mani Sarathy, P. Castaño, J. Gascon, High purity, self-sustained, pressurized hydrogen production from ammonia in a catalytic membrane reactor, Chem. Eng. J. 431 (2022) 134310, https://doi.org/10.1016/j.cej.2021.134310.
- [39] Y. Hayakawa, S. Kambara, T. Miura, Hydrogen production from ammonia by the plasma membrane reactor, Int. J. Hydrogen Energy 45 (56) (2020) 32082–32088, https://doi.org/10.1016/j.jihydene.2020.08.178.
- [40] Navascués, P.; Ruiz-Martín, M.; Regodón, G.; Palmero, A.; Cotrino, J.; González-Elipe, A. R.; Gómez-Ramírez, A. Ammonia to hydrogen conversion in a ferroelectric packed-bed plasma reactor: the effect of a high-permittivity effective medium material. Plasma Process. Polym. n/a (n/a), e70067. doi:https://doi.org /10.1002/ppap.70067.
- [41] A. Bogaerts, X. Tu, J.C. Whitehead, G. Centi, L. Lefferts, O. Guaitella, F. Azzolina-Jury, H.-H. Kim, A.B. Murphy, W.F. Schneider, T. Nozaki, J.C. Hicks, A. Rousseau, F. Thevenet, A. Khacef, M. Carreon, The 2020 plasma catalysis roadmap, J. Phys. D Appl. Phys. 53 (44) (2020) 443001, https://doi.org/10.1088/1361-6463/ab9048.
- [42] E.C. Neyts, K. (Ken) Ostrikov, M.K. Sunkara, A. Bogaerts, Plasma catalysis: synergistic effects at the nanoscale, Chem. Rev. 115 (24) (2015) 13408–13446, https://doi.org/10.1021/acs.chemrev.5b00362.
- [43] N. Wang, H.O. Otor, G. Rivera-Castro, J.C. Hicks, Plasma catalysis for hydrogen production: a bright future for decarbonization, ACS Catal. 14 (9) (2024) 6749–6798, https://doi.org/10.1021/acscatal.3c05434.
- [44] M.R. Shawon, C. Umeojiakor, A. Griffin, J. Aguinaga, J. Wu, D. Patton, Z. Qiang, H. Toghiani, Y. Xiang, Ammonia decomposition over low-loading ruthenium catalyst achieved through "adiabatic" plasma reactor, React. Chem. Eng. 10 (2) (2025) 320–331, https://doi.org/10.1039/D4RE00509K.
- [45] R. De Meyer, Y. Gorbanev, R.-G. Ciocarlan, P. Cool, S. Bals, A. Bogaerts, Importance of plasma discharge characteristics in plasma catalysis: dry reforming of methane vs. ammonia synthesis, Chem. Eng. J. 488 (2024) 150838, https://doi. org/10.1016/j.cej.2024.150838.
- [46] K.S. Conlin, H. Mehrabi, N.D. Parette, M.E. Nichols, H.R. Coridan, Characterizing catalyst function and transformations in the plasma reduction of CO 2 on atomic layer deposition-synthesized catalysts, RSC Applied Interfaces 1 (3) (2024) 552–563, https://doi.org/10.1039/D3LF00271C.
- [47] B. Wang, M. Wang, Z. Fan, C. Ma, S. Xi, L.-Y. Chang, M. Zhang, N. Ling, Z. Mi, S. Chen, W.R. Leow, J. Zhang, D. Wang, Y. Lum, Nanocurvature-induced field effects enable control over the activity of single-atom electrocatalysts, Nat. Commun. 15 (1) (2024) 1719, https://doi.org/10.1038/s41467-024-46175-1.
- [48] M. Purcel, S. Berendts, L. Bonati, S. Perego, A. Müller, M. Lerch, M. Parrinello, M. Muhler, Iron nitride formation and decomposition during ammonia decomposition over a Wustite-based bulk Iron catalyst, ACS Catal. 14 (18) (2024) 13947–13957, https://doi.org/10.1021/acscatal.4c04415.
- [49] X. Zhang, M.S. Cha, Ammonia cracking for hydrogen production using a microwave argon plasma jet, J. Phys. D Appl. Phys. 57 (6) (2023) 065203, https://doi.org/10.1088/1361-6463/ad0988.
- 50] G. Dong, Y. Zhou, P. Ming, Z. Wu, H. Chen, Y. Huang, L. Li, Kinetics-based analysis of the gliding arc plasma assisted ammonia decomposition process towards vehicle on-board applications, Chem. Eng. J. 505 (2025) 159443, https://doi.org/ 10.1016/j.cej.2025.159443.